A Simple Power Estimation With Triple Phase-Shift Control for the Output Parallel DAB DC–DC Converters in Power Electronic Traction Transformer for Railway Locomotive Application

Feng An, Wensheng Song, *Member, IEEE*, Kexin Yang, Shunfeng Yang, *Student Member, IEEE*, and Lei Ma, *Member, IEEE*

***Abstract*— Aimed at the input-independence and output-parallel dual-active-bridge (DAB) dc–dc converters applied to power electronic traction transformer (PETT), this paper proposes a simple power estimation scheme with triple phase-shift control (PES-TPS) to achieve the transmission power balance, dynamic performance improvement, and efficiency optimization, simultaneously. Through executing the current stress optimization (CSO) and introducing the power estimation based on operational parameters, the efficiency of converters can be further improved and the power balance among DAB cells can be achieved over the whole power range without adding extra sensors to sample the output/inductor current of each cell. In addition, the dynamic performance of the adopted converters can be improved by compensating power loss online. Especially, dynamic response of the output voltage can be enhanced under input voltage and load fluctuation conditions. Finally, a comprehensive experimental comparison of CSO with dual phase shift (CSO-DPS), CSO with TPS (CSO-TPS), and the proposed PES-TPS control is conducted in the DAB converters experimental prototype with three cells. The experimental results have confirmed the excellent performance of the proposed PES-TPS control and the correctness of the theoretical analysis.**

***Index Terms*— DC–DC converter, dual active bridge (DAB), dynamic response, efficiency, power balance, power electronic traction transformer (PETT), power estimation.**

I. Introduction

With the growing demand for energy-saving and environmental protection in recent years, the development of new generation high-speed trains trends toward higher speed, higher efficiency, lower running noise, lower weight, and volume. However, the bulky line-frequency transformer becomes one of the major obstacles to increase the power density and reduce the energy consumption [1]. Thus, power electronic traction transformers (PETTs), which are energy-saving, eco-friendly, and high-power density, are regarded as the core traction drive equipment of next-generation high-speed trains [2]–[4].

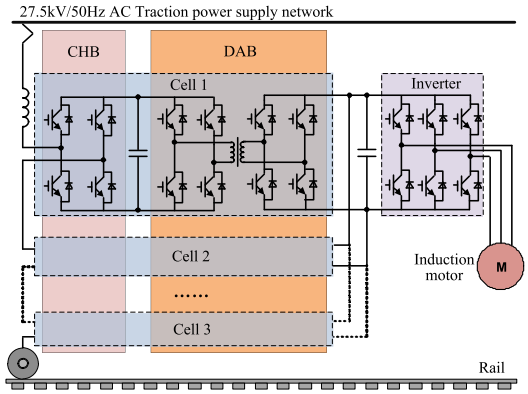

Fig. 1. Topology of the PETT in a train traction drive system.

At present, the most widely adopted PETT railway drive system topology is shown in Fig. 1, which consists of a single-phase cascaded H-bridge (CHB) converter, the input-independent and output-parallel dual-active-bridge (DAB) dc–dc converters, a three-phase inverter, and traction motors [5], [6].

For PETT with the cascaded structure, the basic operation requirement is to balance the output power of each cell. However, in practical application, the unbalance issue of transmission power is inevitable due to circuit parameters' mismatch [7]. Furthermore, the unbalanced transmission power may cause excessive current stress, low efficiency, and even breakdown of insulated-gate bipolar transistor devices [8].

In order to balance the output dc voltages of the front-end CHB converter and real power of the output-parallel DAB converters, She *et al.* [9] propose a simple and effective voltage and power balancing solution based on the single-phase d–q model. However, the additional inductor current sensor needed in each DAB cell greatly increases the system cost.

Manuscript received April 2, 2018; revised July 6, 2018 and August 30, 2018; accepted October 5, 2018. Date of publication October 15, 2018; date of current version March 19, 2019. This work was supported in part by the National Natural Science Foundation of China under Project 61733015 and in part by the National Key R&D Program of China under Project 2017YFB1200901. *(Corresponding author: Wensheng Song.)*

The authors are with the School of Electrical Engineering, Southwest Jiaotong University, Chengdu 610031, China (e-mail: anfengswjtu@163.com; songwengsheng@163.com).

Digital Object Identifier 10.1109/TTE.2018.2876057

Furthermore, a power balancing scheme without sensing the inductor currents for PETTs is discussed in [9], where a real power component of the duty cycle controller is applied to CHB converters and a feed-forward controller is used for DAB converters. Although this scheme does not use for inductor current sensors, the efficiency of the output-parallel DAB converters is relatively low because of the adopted single phase-shift (SPS) control. The transmission power of the DAB converter in the SPS control is strongly related to the storage inductance that will lead to high current stress and low efficiency when the voltage transfer ratio deviates far from one [10]–[12].

In order to improve the transfer efficiency of DAB converters, various advanced phase-shift modulation methods have been proposed [13]–[15]. Specifically, some optimized operation schemes with the dual-phase-shift (DPS) control for DAB converters are reported in [16] and [17] to achieve high efficiency over a wide power range. However, these optimization schemes are too complex to be realized in real-time digital microprocessors. Furthermore, a current stress optimization with DPS (CSO-DPS) control scheme is proposed in [18] to reduce current stress through the cost function minimization. This control method can minimize current stress online according to the operating conditions of converters, but the obtained minimum current stress is not the global optimal solution because there are only two controllable freedoms in the DPS control. In order to further reduce the current stress, a CSO and soft-switching operation scheme with triple phase-shift (TPS) control for DAB converters is proposed in [19] to minimize the current stress and achieve full soft-switching operation with the required power transmission over the whole load range. In this scheme, the closed-form solutions for the global optimal operation parameters are derived with the Karush–Kuhn–Tucker (KKT) condition, which is an effective method to solve the extreme optimization problem with inequality constraint. But the obtained optimal solution is very complex, which is not suitable to be extended into DAB converters with the cascaded structure. Subsequently, Hou *et al.* [20] propose a simple CSO scheme with TPS (CSO-TPS) control through the Lagrange multiplier method (LMM). However, all the optimized phase-shift ratios in the CSO-TPS scheme are obtained through a proportional–integrator (PI) controller. Thus, these schemes cannot be extended into the output-parallel DAB converters to balance the transfer power of each cell. In addition, a dynamic response of the output voltage in these existed CSO-TPS schemes is a little bit slow.

Fast dynamic response for DAB converters in PETT is very important because there always exists twice-grid-frequency ripple in the intermediate dc capacitor voltages, which may further cause the beat frequency phenomenon of the traction motor [21]. In [22]–[24], the small-signal model of the DAB converter in the SPS control is developed, and the dynamic characteristic of DAB converters is studied. In [25] and [26], an adaptive dynamic controller is designed through utilizing a dynamic linearized harmonic model, which can improve the dynamic performance by adjusting the PI gains online. However, the linearized harmonic model is relatively complex and difficult to be implemented in the digital controller of the

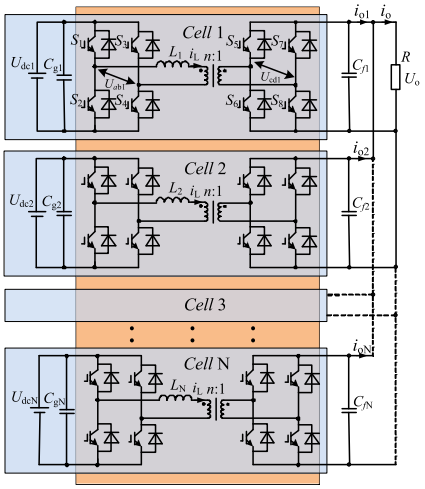

Fig. 2. Equivalent input-independent output-parallel DAB dc–dc converters in PETT.

output-parallel multiple DAB converters. Furthermore, on the basis of the SPS control, a virtual direct power control scheme is reported in [27], which can achieve nonovershoot and fast transient response for the output voltage in load or input voltage step-change and startup stage. However, the performance of the virtual direct power control under other phase-shift schemes needs to be investigated.

Aimed at dealing with the aforementioned issues for the output-parallel DAB converters in PETT, a simple power estimation scheme with TPS (PES-TPS) control is proposed in this paper. First, the CSO in the TPS control is introduced to improve the transfer efficiency of converters. Then, the transmission power balance in the CSO-DPS and CSO-TPS control schemes is analyzed in detail. Subsequently, the power estimation based on operational parameters is proposed, which can enhance the dynamic response of the output voltage and balance the transmission power of each cell. Compared with the existing optimized schemes for DAB converters, the salient features of the proposed PES-TPS control can be summarized as follows.

1) The integrated PES-TPS control based on operational parameters is easily extended and applied to output-parallel DAB converters consisting of N cells.
2) The transmission power balance over the whole power range is achieved, without the addition of extra sensors to sample the output/inductor current of each cell.
3) Dynamic response of the output voltage is obviously enhanced, under the input voltage fluctuation and load disturbance conditions.
4) Efficiency of the entire output-parallel DAB converters is improved.

II. Analysis of Triple Phase-Shift Control

When the dc capacitor voltages of the front CHB converter are balanced, the DAB converters can be regarded as the input-independent output-parallel connection. Fig. 2 shows the equivalent circuit consists of N DAB cells, where U_{dci} represents the input voltage of the ith cell; C_{gi} and C_{fi} represent the input-side capacitor and output-side capacitor of

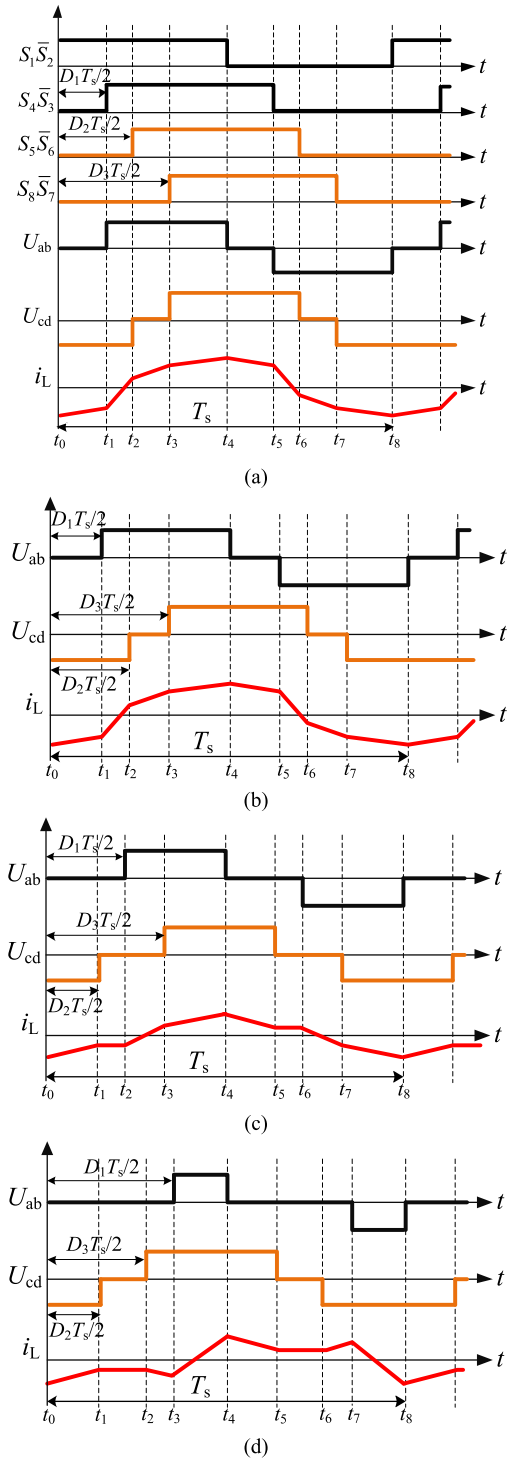

Fig. 3. Main waveforms of switching sequences, voltage and current waveforms in TPS control. (a) Switching sequences. (b) $0 \le D_1 \le D_2 \le D_3 \le 1$. (c) $0 \le D_2 \le D_1 \le D_3 \le 1$. (d) $0 \le D_2 \le D_3 \le D_1 \le 1$.

the ith cell, respectively; U_o is the output voltage; L_i is the auxiliary inductor of the ith cell; U_{abi} and U_{cdi} represent the ac output voltage of the primary and secondary H-bridge; i_o is the load current; i_{oi} represents the output current of the ith cell; R is the equivalent load resistor; and turn ratio of the isolated transformer is n: 1.

Fig. 3(a) shows the main switching sequences, voltage and current waveforms of a DAB dc–dc converter in the TPS control, where i_L is the inductor current; T_s represents a switching period; D_1T_s is the phase-shift ratio between switches S_1 and S_4 (S_1 ahead of S_4); D_2T_s is the phase-shift ratio between switches S_1 and S_5 (S_1 ahead of S_5); and D_3T_s is the phase-shift ratio between switches S_1 and S_8 (S_1 ahead of S_8). Obviously, all the phase-shift ratios in one DAB converter cell are referred to the same modulated signal S_1, which is very convenient to be implemented in digital microprocessors [20]. Moreover, phase-shift angle of the modulated reference signal in every DAB cell is set as $360°/N$ to minimize the output voltage ripple [4].

It is clear that there are three independent phase-shift ratios D_1, D_2, and D_3 in the TPS control, so the relationship between the phase-shift ratios can be divided into six conditions. However, no matter the phase-shift ratio D_2 is larger or smaller than D_3, the same waveforms of U_{ab}, U_{cd}, and i_L can be obtained, and the transmission power is identical [20]. Thus, the phase-shift ratio D_2 can be configured less than D_3 to simplify the phase-shift ratio conditions. The main waveforms of voltage and current in the TPS control are shown in Fig. 3(b)–(d).

According to Fig. 3, the averaging power and current stress of each DAB cell with the TPS control can be expressed as

$$\begin{cases} P = \dfrac{1}{T_s}\displaystyle\int_0^{T_s} U_{ab} i_L(t)dt \\ I_p = \max\ \{|i_L(t)|\}. \end{cases} \tag{1}$$

Taking the ith DAB cell as an example, assuming the voltage transfer ratio $k_i = U_{dci}/nU_o$, and $k_i \ge 1$ (the condition $k_i < 1$ can be derived similarly), the averaging power and current stress in the TPS control can be derived as [20]

$$\begin{cases} P_i = \begin{cases} \dfrac{nU_{dci}U_o}{4fL_i}\big(-D_{i1}+D_{i2}+D_{i3}-D_{i1}^2-D_{i2}^2 \\ \quad -D_{i3}^2+D_{i1}D_{i2}+D_{i1}D_{i3}\big)(D_{i1} \le D_{i2} \le D_{i3} \le 1) \\ \dfrac{nU_{dci}U_o}{4fL_i}\big(-D_{i1}+D_{i2}+D_{i3}-D_{i1}D_{i2} \\ \quad -D_{i3}^2+D_{i1}D_{i3}\big)(D_{i2} \le D_{i1} \le D_{i3} \le 1) \\ \dfrac{nU_{dci}U_o}{4fL_i}\big(-D_{i1}+D_{i2}+D_{i3}-D_{i1}D_{i2} \\ \quad +D_{i1}^2-D_{i1}D_{i3}\big)(D_{i2} \le D_{i3} \le D_{i1} \le 1) \end{cases} \\ I_{p_i} = \dfrac{nU_o}{4fL_i}[D_{i2}+D_{i3}-1+k_i(1-D_{i1})] \end{cases} \tag{2}$$

where $f = 1/T_s$ represents the switching frequency.

In order to simplify the calculation, the rated power and rated current stress of the ith DAB converter can be defined as

$$\begin{cases} P_{N_i} = \dfrac{nU_{dci}U_o}{8fL_i} \\ I_{N_i} = \dfrac{P_{N_i}}{U_{dci}} = \dfrac{nU_o}{8fL_i} \end{cases} \tag{3}$$

where P_{Ni} is the rated output power and I_{Ni} is the rated current stress in the TPS control.

Furthermore, the unified averaging power p_i and current stress in the TPS control can be derived as

$$\begin{cases} p_i = \begin{cases} 2\big(-D_{i1}+D_{i2}+D_{i3}-D_{i1}^2-D_{i2}^2-D_{i3}^2 \\ +D_{i1}D_{i2}+D_{i1}D_{i3}\big)(D_{i1}\le D_{i2}\le D_{i3}\le 1) \\ 2\big(-D_{i1}+D_{i2}+D_{i3}-D_{i1}D_{i2}-D_{i3}^2 \\ +D_{i1}D_{i3}\big)(D_{i2}\le D_{i1}\le D_{i3}\le 1) \\ 2\big(-D_{i1}+D_{i2}+D_{i3}-D_{i1}D_{i2}+D_{i1}^2 \\ \quad -D_{i1}D_{i3}\big)(D_{i2}\le D_{i3}\le D_{i1}\le 1) \end{cases} \\ i_{p_i} = 2[D_{i2}+D_{i3}-1+k_i(1-D_{i1})]. \end{cases} \tag{4}$$

III. Current Stress Optimization in TPS Control

Generally, typical optimization problems can be divided into the following three categories.

1) *Unconstrained Extreme Optimization Problem:* This kind of problem is the simplest case, and the solution is usually the derivation of the cost function to the variables [18].
2) *Extreme Optimization Problem With Equivalent Constraint:* This kind of problem cannot be solved through the derivation of the cost function, because the solution is limited by the equivalent constraint. Thus, LMM is widely used to solve this kind of problems. LMM can obtain the optimal solutions through searching the relationship between cost function and the equivalent constraint with the Lagrange multiplier [14], [20].
3) *Extreme Optimization Problem With Inequality Constraint:* This kind of problem is a little bit complex, and KKT condition are an effective method to solve the problems [19]. Besides, there are other advanced optimizations, particularly metaheuristic, such as genetic algorithm [28], [29] and ant colony optimization [30], which are available to solve the optimization problem with constraint condition. But it should be noticed that most of the algorithms need the time-consuming trial-and-error tuning procedure (i.e., iterative calculation) to achieve the satisfactory performance, which brings heavy computational burden to the controller, especially for the cascaded converters consisting of N cells.

From the mathematical perspective, searching the optimal phase-shift ratio combination at the desired transmission power to minimize the current stress belongs to the extreme optimization problem with equivalent constraint, which can be formulated as

$$\begin{cases} \min\limits_{D_{i1},\ D_{i2},\ D_{i3}} i_{pi}(D_{i1}, D_{i2}, D_{i3}) \\ \quad \text{s.t. } p_i(D_{i1}, D_{i2}, D_{i3}) = p_i^*, \quad i = 1, 2, \cdots, N. \end{cases} \tag{5}$$

Specifically, the equivalent constraint is the desired transmission power; the optimized goal is the current stress of converters (i.e., minimize the current stress subjecting to the desired transmission power); and the optimization variables are the phase-shift ratios D_{i1}, D_{i2}, and D_{i3}. Thus, LMM is adopted to achieve CSO in this section [17].

First, the Lagrange function is defined to describe the relationship between the current stress (objective function) and transmission power (equivalent constraint) as follows:

$$E_i = i_{p_i} + \lambda_i(p_i - p_i^*) \tag{6}$$

where E_i is the Lagrange function and λ_i is the Lagrange multiplier.

In order to minimize the current stress, the relationship between the optimized phase-shift ratios can be derived by taking a derivative with respect to phase-shift ratios D_{i1}, D_{i2}, and D_{i3} as

$$\begin{cases} \dfrac{\partial E_i}{\partial D_{i1}} = 0 \\ \dfrac{\partial E_i}{\partial D_{i2}} = 0 \\ \dfrac{\partial E_i}{\partial D_{i2}} = 0. \end{cases} \tag{7}$$

Substituting (4) and (6) into (7), the relationship between the phase-shift ratios D_{i1}, D_{i2}, and D_{i3} can be depicted as

$$\begin{cases} D_{i2} = \begin{cases} (k_i-1)(1-D_{i1}) \left(0 \le p_i \le \dfrac{2k_i-2}{k_i^2}\right) \\ \dfrac{(2-k_i)(1-D_{i1})}{2(k_i-1)} + \dfrac{2k_i-3}{2(k_i-1)} \left(\dfrac{2k_i-2}{k_i^2} < p_i \le 1\right) \end{cases} \\ D_{i3} = \begin{cases} D_{i1} \left(0 \le p_i \le \dfrac{2k_i-2}{k_i^2}\right) \\ \dfrac{(2-k_i)(1-D_{i1})}{2(k_i-1)} + \dfrac{2k_i-3}{2(k_i-1)} \left(\dfrac{2k_i-2}{k_i^2} < p_i \le 1\right). \end{cases} \end{cases} \tag{8}$$

Furthermore, combining (4) with (8), the optimized phase-shift ratios D_{i1}, D_{i2}, and D_{i3} of the ith DAB dc–dc converter can be expressed with respect to the voltage transfer ratio k_i and unified transmission power p_i as

$$\begin{cases} \begin{cases} D_{i1} = 1 - \dfrac{\sqrt{2p_i(k_i-1)}}{2k_i-2} \\ D_{i2} = \sqrt{\dfrac{p_i(k_i-1)}{2}} \left(0 \le p_i \le \dfrac{2k_i-2}{k_i^2}\right) \\ D_{i3} = 1 - \dfrac{\sqrt{2p_i(k_i-1)}}{2k_i-2} \end{cases} \\ \begin{cases} D_{i1} = (k_i-1)\sqrt{\dfrac{1-p_i}{k_i^2-2k_i+2}} \\ D_{i2} = \dfrac{1}{2} - \dfrac{2-k_i}{2}\sqrt{\dfrac{1-p_i}{k_i^2-2k_i+2}} \left(\dfrac{2k_i-2}{k_i^2} < p_i \le 1\right) \\ D_{i3} = \dfrac{1}{2} - \dfrac{2-k_i}{2}\sqrt{\dfrac{1-p_i}{k_i^2-2k_i+2}}. \end{cases} \end{cases} \tag{9}$$

Subsequently, Substituting (9) into (4), the minimum current stress of the ith DAB converter in the TPS control can be

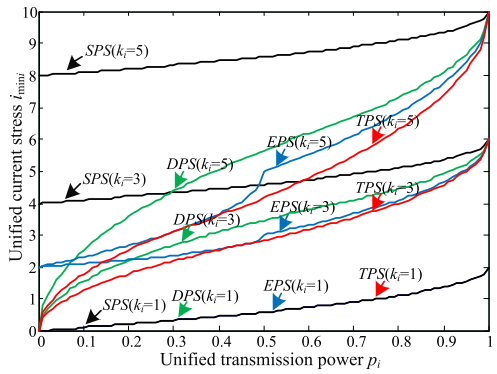

Fig. 4. Relation curves of the unified current stress in SPS, DPS, EPS, and TPS control schemes with respect to the unified transmission power and the voltage transfer ratio.

obtained as

$$i_{\min_i} = \begin{cases} 2\sqrt{2p_i(k_i-1)} \left(0 \le p_i \le \dfrac{2k_i-2}{k_i^2}\right) \\ 2k_i - 2\sqrt{(1-p_i)(k_i^2-2k_i+2)} \left(\dfrac{2k_i-2}{k_i^2} < p_i \le 1\right). \end{cases} \tag{10}$$

In order to compare the obtained minimum current stress of DAB converters under SPS control, DPS control [18], EPS control [14], and TPS control schemes clearly, Fig. 4 shows the relation curves of unified current stress in SPS, DPS, EPS, and TPS control schemes with respect to the unified transmission power and the voltage transfer ratio.

Clearly, the current stress of DAB converters in the SPS control scheme is the largest, and it increases sharply. Meanwhile, the current stress can be reduced effectively in DPS and EPS controls. Moreover, the current stress of DAB converters in the TPS control scheme is the smallest over full power range.

There are usually two ways to execute the existing CSO schemes [14], [18], [20] after obtaining the optimized phase-shift ratios. The first mode is that one of the optimized phase-shift ratios is obtained from a PI controller for the output voltage regulation. The other optimized phase-shift ratios are obtained according to the transfer ratio k_i and power p_i as in (9). It is worth noting that the optimized phase-shift ratio obtained from the PI controller must be monotonically increasing or decreasing with the unified transmission power. Otherwise, the optimized phase-shift ratio cannot be obtained with the PI controller. Meanwhile, the unified transmission power p_i in (9) is replaced with the unified output power, which is deduced as follows:

$$p_i = \frac{U_o i_o}{N P_{N_i}} = \frac{8 f L_i i_o}{n N U_{dci}}. \tag{11}$$

A typical example of the first mode is the CSO-DPS control scheme, and the optimized phase-shift ratio estimation in the

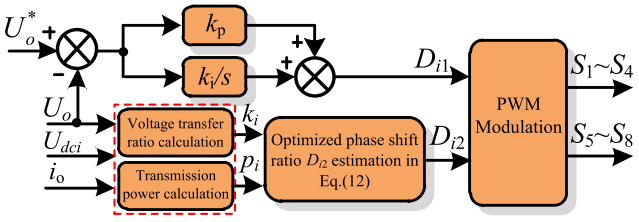

Fig. 5. Block diagram of the CSO-DPS control scheme for the ith DAB converter.

CSO-DPS control scheme [18] can be expressed as

$$\begin{cases} \begin{cases} D_{i1} = (k_i-1)\sqrt{\dfrac{1-p_i}{2(k_i^2-2k_i+3)}} \\ D_{i2} = \dfrac{1}{2} - \sqrt{\dfrac{1-p_i}{2(k_i^2-2k_i+3)}} \end{cases} \left(\dfrac{k_i^2+2k_i-3}{2k_i^2} < p_i \le 1\right) \\ \begin{cases} D_{i1} = 1 - \sqrt{\dfrac{p_i(k_i-1)}{2(k_i+3)}} - \sqrt{\dfrac{2p_i}{(k_i-1)(k_i+3)}} \\ D_{i2} = \dfrac{p_i(k_i-1)}{2(k_i+3)} \end{cases} \left(0 \le p_i \le \dfrac{k_i^2+2k_i-3}{2k_i^2}\right). \end{cases} \tag{12}$$

The block diagram of the CSO-DPS control scheme for the ith DAB converter is shown in Fig. 5, where the optimized phase-shift ratio D_{i1} is obtained from the PI controller, and the optimized phase-shift ratio D_{i2} is estimated based on (12).

The second mode is that one of the optimized phase-shift ratios, which is monotonically varying with respect to the unified transmission power, is also obtained through the PI controller. The other optimized phase-shift ratios are derived from the relationship between the optimized phase-shift ratios as in (8). A typical example of the second mode is the CSO-TPS control scheme [20].

According to (9), it can be noticed that D_{i1} is monotonically decreasing along with the unified transmission power p_i. Meanwhile, D_{i2} is first increasing and then decreasing along with the unified power p_i when voltage transfer ratio $k_i > 2$; if $k_i < 2$, D_{i3} is first decreasing and then increasing along with the unified transmission power p_i. Only D_{i1} is monotonically decreasing along with the unified transmission power p_i. Thus, (9) can be rewritten as

$$\begin{cases} \begin{cases} D_{i1} = 1 - p_c \\ D_{i2} = (k_i-1)p_c \left(0 \le p_c \le \dfrac{1}{k_i}\right) \\ D_{i3} = 1 - p_c \end{cases} \\ \begin{cases} D_{i1} = 1 - p_c \\ D_{i2} = \dfrac{(2-k_i)p_c + 2k_i - 3}{2(k_i-1)} \left(\dfrac{1}{k_i} < p_c \le 1\right) \\ D_{i3} = \dfrac{(2-k_i)p_c + 2k_i - 3}{2(k_i-1)} \end{cases} \end{cases} \tag{13}$$

where p_c is the output of the PI controller for the output voltage regulation.

Although all the above two executing approaches can minimize the current stress, the dynamic response is a little bit poor

because the optimized phase-shift ratio estimation is strongly relative to the PI controller. For the optimized phase-shift ratio obtained through the PI controller of each DAB cell, its value is always the same even if the storage inductances in the DAB cells are unequal, which leads to the unbalanced transmission power. Thus, the second executing approach cannot be extended into the output-parallel converters to balance the transmission power because all the optimized phase-shift ratios are obtained through the PI controller. Similarly, the power balance can only be partially realized in the first executing approach because one of the optimized phase-shift ratios is obtained from the PI controller.

IV. Proposed Power Estimation Scheme With Triple Phase-Shift Control

According to the aforementioned analysis, the obtained optimized phase-shift ratios in (9) cannot be applied to the output-parallel DAB converters directly due to the self-power-characteristic of the adopted converters. Instead, the PI controller is usually utilized to control one or all phase-shift ratios to achieve minimum CSO. It not only weakens the dynamic performance of the converter to a certain extent but also leads to the unbalanced transmission power among DAB cells in PETT.

In order to balance the transmission power over full power range, enhance the dynamic response, and improve the efficiency performance for input-independent output-parallel DAB converters in PETT, a simple PES-TPS control (PES-TPS) is proposed in this paper, where the power loss compensation solution is adopted to enhance the dynamic response of the output voltage. In the traditional CSO schemes, the unified transmission power is replaced by the unified output power directly. However, in practical applications, the input power is not equal to the output power due to power losses. Thus, the desired output power expressed with the arithmetic product of the desired output voltage U_{o}^{*} and current i_{o}^{*} cannot completely reflect the desired transmission power, and a power compensation component should be added to compensate this power difference. So, the estimated transmission power of the output-parallel DAB converters can be described as

$$P_e = \left(U_o^* + \Delta U_o\right) i_o^* = U_o^* i_o^* + \Delta U_o i_o^* \tag{14}$$

where $\Delta U_{\mathrm{o}} i_{\mathrm{o}}^{*}$ is the power compensation component and ΔU_{o} can be obtained through the output voltage PI controller. The desired output current can be estimated online as [27]

$$i_o^* = \frac{U_o^*}{U_o} i_o. \tag{15}$$

Substituting (15) into (14) yields

$$P_e = \left(U_o^* + \Delta U_o\right) \frac{U_o^*}{U_o} i_o. \tag{16}$$

For the output-parallel DAB dc–dc converters consisting of N cells in PETT, in order to balance the transmission power over full power range, the output current of each module should meet

$$i_{o1} = i_{o2} = \cdots = i_{oi} = \cdots = i_{oN} = \frac{i_o}{N}. \tag{17}$$

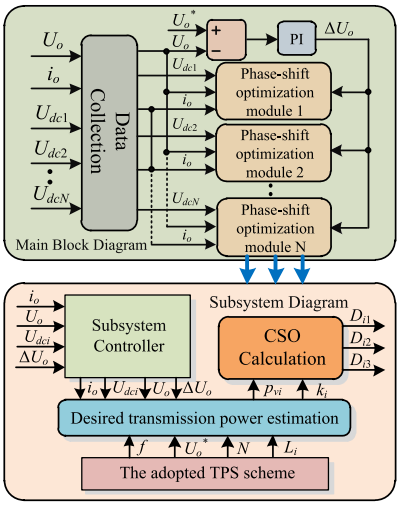

Fig. 6. Block diagram of the PES-TPS control for the input-independent output-parallel DAB converters.

Combined (3), (16), and (17), the estimated power of the ith cell with the PES-TPS control is obtained as

$$p_{e_i} = \frac{8 f L_i (U_o^* + \Delta U_o) U_o^* i_o}{n N U_{dci} U_o^2} \tag{18}$$

where p_{ei} is the estimated power of the ith cell.

Furthermore, the proposed PES-TPS control for the output-parallel DAB dc–dc converters in PETT can be realized through the following steps.

1) The input voltage U_{dci}, the output voltage U_o, and the load current i_o of converters are sampled by the voltage/current sensors.
2) The voltage transfer ratio k_i is calculated based on the input and output voltages, and the desired power p_{ei} of the ith cell is estimated from (18).
3) The optimized phase-shift ratios D_{i1}, D_{i2}, and D_{i3} of the ith DAB dc–dc converter can be obtained from (9).
4) The driving pulse signals of each DAB cell are generated from the TPS pulse modulator stage according to the optimized phase-shift ratios.

The block diagram of the PES-TPS control for the output-parallel DAB converters in PETT is shown in Fig. 6.

V. Experiments

A scaled-down laboratory prototype consisting of three output-parallel DAB converters is designed, and the aforementioned theoretical analysis has been verified in this section. Fig. 7 shows a photograph of the laboratory platform.

The parameters of the adopted experimental platform are listed in Table I.

A comprehensive comparison consisting of the CSO-DPS control [18], the CSO-TPS control [20], and the proposed PES-TPS controls are conducted in this section. The experimental comparison mainly includes four parts: first, dynamic responses of the DAB converters with CSO-DPS, CSO-TPS, and PES-TPS controls are compared under the load and input voltage step-change conditions. Then, the transmission power

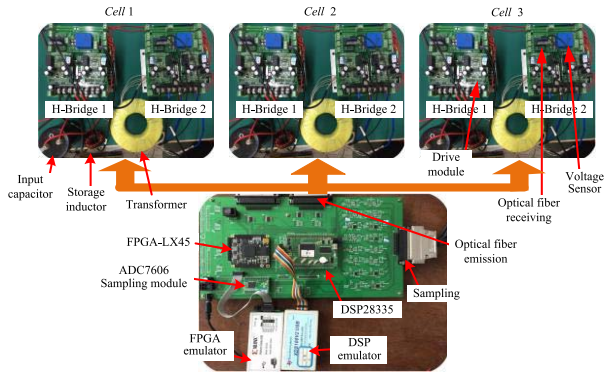

Fig. 7. Photograph of the scaled-down laboratory platform with three DAB modules.

TABLE I

PARAMETERS OF THE DAB CONVERTER EXPERIMENTAL PLATFORM WITH THREE MODULES

Parameters	Value
Turn ratio of transformers	n=1
Switching frequency	f= 10kHz
Inductor of Cell 1	L_1=184μH
Inductor of Cell 2	L_2=112μH
Inductor of Cell 3	L_3=226.7μH
Input-side capacitor	C_{g1}= C_{g2}= C_{g3}=1.12mF
Output-side capacitor	C_{f1}= C_{f2}= C_{f3}=1.12mF
Load resistor	R=10/20/30Ω

balancing ability of the output-parallel DAB converters under the PES-TPS control is presented. Subsequently, the convergence between the practical phase-shift ratios/current stress and theoretical phase-shift ratios/current stress is verified. The current stress and efficiency of DAB converters under CSO-DPS, CSO-TPS, and PES-TPS controls are shown and compared. Finally, the computational burdens of the controller in CSO-DPS, CSO-TPS, and PES-TPS controls are compared.

A. Experimental Comparison of Dynamic Response

With the input voltage $U_{dc1} = U_{dc2} = U_{dc3} = 80$ V and the desired voltage $U_o^* = 70$ V, Figs. 8 and 9 show the experimental waveforms of the output-parallel DAB converters under CSO-DPS, CSO-TPS, and PES-TPS controls when the load resistance steps between 5 and 30 Ω. It is clear that the maximum settling time of the output voltage in the CSO-TPS scheme is about 1120 ms, and the largest voltage fluctuation is about 67 V. In the CSO-DPS scheme, the output voltage fluctuation of converters is suppressed significantly, but the settling time of the output voltage is still very long (over 650 ms). By contrast, it can be seen that the output voltage fluctuation is very small, and the output voltage almost keeps constant under the proposed PES-TPS control no matter how the load resistor steps change. Meanwhile, the settling time of the output voltage in the PES-TPS control is significantly decreased to about 52 ms.

With the desired voltage $U_o^* = 70$ V and the load resistor $R = 10$ Ω, Figs. 10 and 11 show the waveforms of converters under three controls when the input voltage steps change between 70 and 90 V. Clearly, the settling time of the output voltage in the CSO-TPS control scheme is the longest, over 210 ms. For the CSO-DPS control scheme, the voltage fluctuation is reduced significantly, but the settling time of the output voltage is only slightly shorter, about 190 ms. However, it is clear that the output voltage almost remains constant during the input voltage step-change processes in the PES-TPS control. Thus, the proposed PES-TPS control can achieve the fast dynamic response for the input-independent output-parallel DAB converters.

B. Experimental Comparison of Power Balance

With the input voltage $U_{dc1} = U_{dc2} = U_{dc3} = 110$ V, the desired voltage $U_o^* = 100$ V, and the load resistor $R = 10$ Ω, Fig. 12 shows the experimental waveforms of output current in each cell when the optimized scheme is switched from the CSO-TPS control to the PES-TPS control. In the CSO-TPS control scheme, it is clear that the output currents of DAB cells are unequal, and the output current in cell 2 is larger than the other two cells because of its smaller inductance. For the DAB cell with larger transmission power, the current stress is also larger, which causes efficiency reduction. However, the proposed PES-TPS control can achieve the power balance instantly even though the storage inductance of the individual DAB cell is different from each other.

With the input voltage $U_{dc1} = U_{dc2} = U_{dc3} = 110$ V, the desired voltage being $U_o^* = 100$ V, and the load resistor changing between 20 and 10 Ω, the transient waveforms of the output current in each cell in CSO-DPS, CSO-TPS, and PES-TPS controls are shown in Fig. 13. Compared to CSO-TPS control and CSO-DPS control schemes, it is clear that the proposed PES-TPS control can always balance the transmission power in each cell at different power levels, and the averaging output currents of all cells are always equal.

C. Experimental Comparison of Current Stress and Efficiency

With the desired voltage $U_o^* = 80$ V and the load resistor $R = 20$ Ω, Fig. 14(a) shows the curves of the optimized phase-shift ratios in theory and real with respect to the input voltage in the PES-TPS control. It can be seen that the practical optimized phase-shift ratios are converged to the theoretical values although there is a small difference caused by the dead time, the switch parameters, and the perform precision of microcontroller. Meanwhile, Fig. 14(b) shows the relation curves of current stress in theory and real versus input voltage in the PES-TPS control. It can be observed that the practical current stress of converters is almost consistent with the theoretical value, which further proves the correctness of the theoretical analysis.

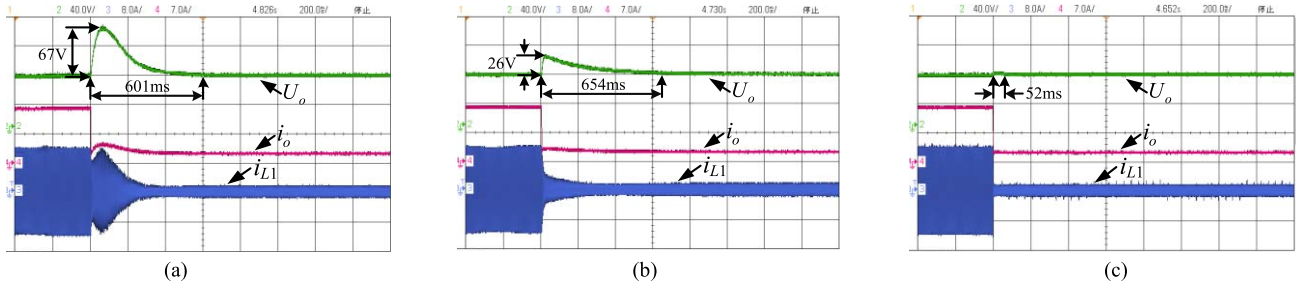

Fig. 8. Experimental waveforms of DAB converters in three controls when the load resistor steps up from 5 to 30 Ω (U_o: 40 V/div, i_{L1}: 8 A/div, i_o: 7 A/div, and time: 200 ms/div). (a) CSO-TPS. (b) CSO-DPS. (c) PES-TPS.

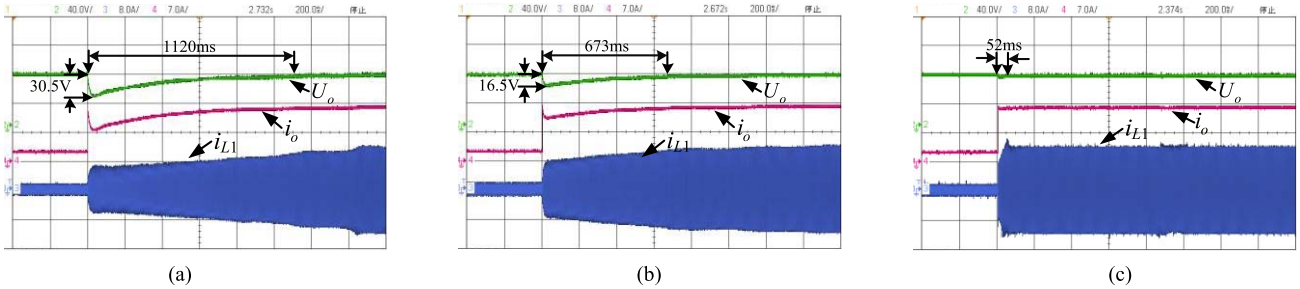

Fig. 9. Experimental waveforms of DAB converters in three controls when the load resistor steps down from 30 to 5 Ω (U_o: 40 V/div, i_{L1}: 8 A/div, i_o: 7 A/div, and time: 200 ms/div). (a) CSO-TPS. (b) CSO-DPS. (c) PES-TPS.

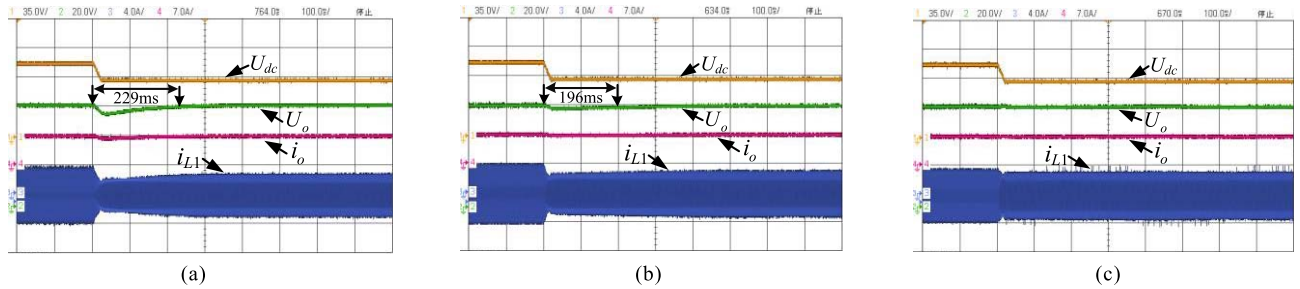

Fig. 10. Experimental waveforms of DAB converters in three control schemes when the input voltage steps down from 90 to 70 V (U_{dc}: 35 V/div, U_o: 20 V/div, i_{L1}: 4 A/div, i_o: 7 A/div, and time: 100 ms/div). (a) CSO-TPS. (b) CSO-DPS. (c) PES-TPS.

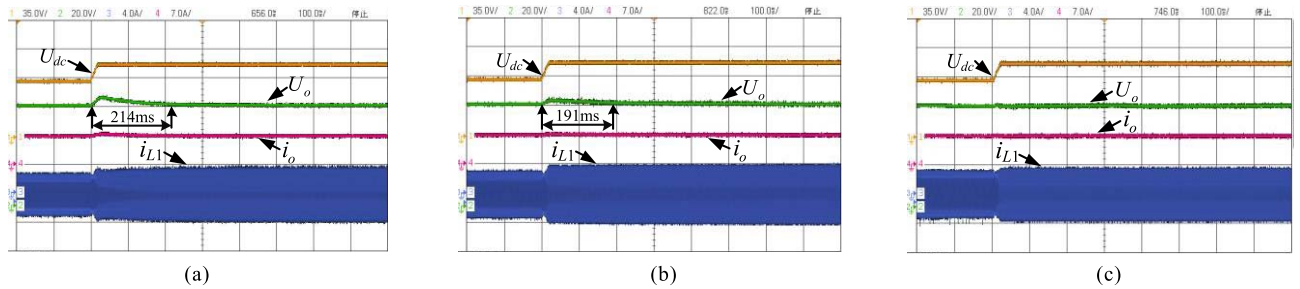

Fig. 11. Experimental waveforms of DAB converters in three control schemes when the input voltage steps up from 70 to 90 V (U_{dc}: 35 V/div, U_o: 20 V/div, i_{L1}: 4 A/div, i_o: 7 A/div, and time: 100 ms/div). (a) CSO-TPS. (b) CSO-DPS. (c) PES-TPS.

With the input voltage $U_{dc1} = U_{dc2} = U_{dc3} = 150$ V, the desired voltage $U_o^* = 80$ V, and the load resistor $R = 30$ Ω, the ac output voltage and inductor current experimental waveforms of DAB cell 1 under three control schemes are shown in Fig. 15. In the CSO-DPS control, the current stress is about 4.6 A. The CSO-TPS control scheme can reduce current stress effectively to 4.3 A. However, the unbalanced transmission power leads to a higher current stress of cell 1. In the proposed PES-TPS control, the transmission power of each cell is balanced, which can further reduce the current stress to 3.9 A.

With the desired voltage $U_o^* = 80$ V and the load resistor $R = 20$ Ω, Fig. 16(a) and (b) shows the current stress and the

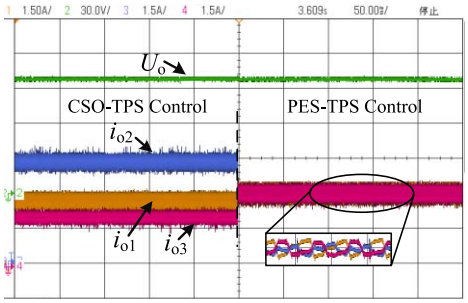

Fig. 12. Experimental waveforms of output current in each DAB cell when the control scheme is switched from the CSO-TPS scheme to the PES-TPS scheme (i_{o1}: 1.5 A/div, U_o: 30 V/div, i_{o2}: 1.5 A/div, i_{o3}: 1.5 A/div, and time: 50 ms/div).

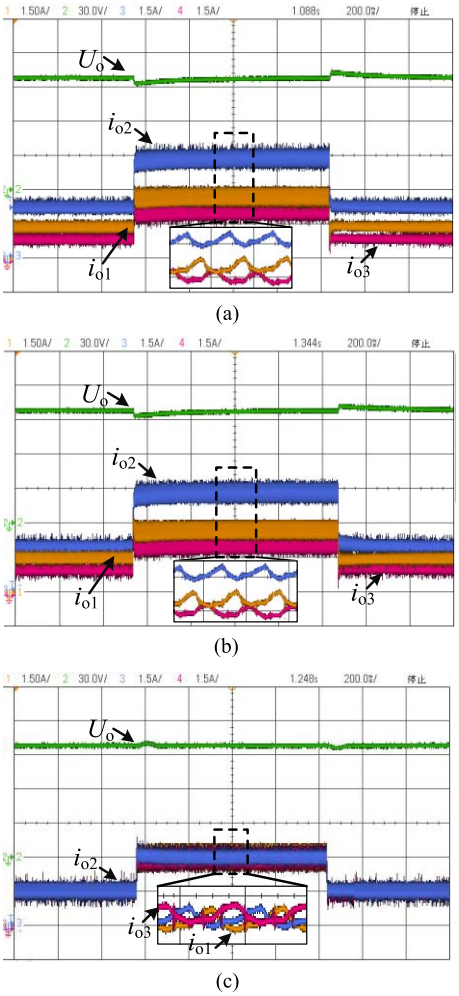

Fig. 13. Experimental waveforms of the output current in each cell under (a) CSO-DPS, (b) CSO-TPS, and (c) PES-TPS controls when the load resistor steps between 20 and 10 Ω (i_{o1}: 1.5 A/div, U_o: 30 V/div, i_{o2}: 1.5 A/div, i_{o3}: 1.5 A/div, and time: 200 ms/div).

efficiency of the output-parallel DAB dc–dc converters with respect to the input voltage in SPS, CSO-DPS, CSO-TPS, and PES-TPS controls. It can be seen that the current stress of DAB converters in the SPS control is very large, which leads to an efficiency decreasing to as low as 64.8%. In the CSO-DPS

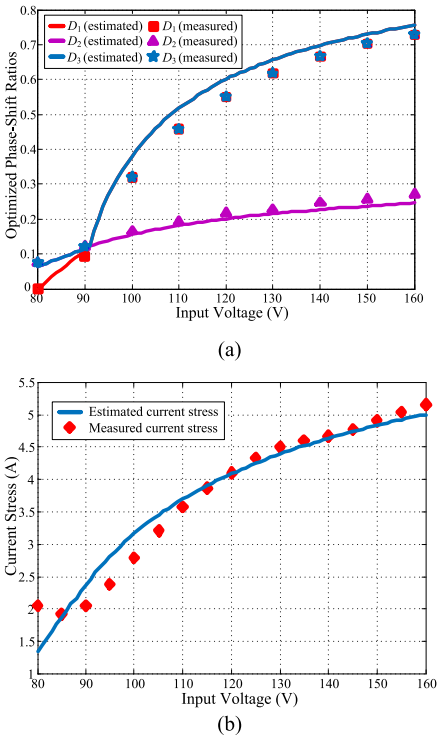

Fig. 14. Curves of (a) optimized phase-shift ratios and (b) current stress in theory and real with respect to the input voltage in the PES-TPS control.

control scheme, the current stress is reduced effectively, especially at high voltage transfer ratios. But the minimum current stress in the CSO-DPS control scheme is not the optimal solution because there are only two controllable freedoms in the DPS control, and the current stress can be further reduced in the CSO-TPS control scheme. Compared to the CSO-DPS control scheme, the converter efficiency in the CSO-TPS control scheme can be boosted up by 4.2% at most. However, the unbalanced power causes larger current stresses in partial cells, and it will further lead to the decrease of efficiency of the whole system. In the proposed PES-TPS control, the current stress of converters is further reduced by balancing the power among cells, and the efficiency can be slightly improved.

In addition, Fig. 16(c) shows the experimental waveforms of efficiency versus power in SPS, CSO-DPS, CSO-TPS, and PES-TPS controls when the voltage transfer ratio is $k = 2$. Clearly, the PES-TPS control can further increase the converter efficiency, compared to the other three control schemes, especially under light load condition.

D. Experimental Comparison of Computational Burden

In order to compare the computational burden of three optimized schemes specifically, Fig. 17 shows the experimental comparison of real-time implementation details under CSO-DPS, CSO-TPS, and PES-TPS controls during a sampling interval. From Fig. 17, the main difference among three schemes is the optimized phase-shift ratio calculation. The computing time of the optimized phase-shift ratios in the

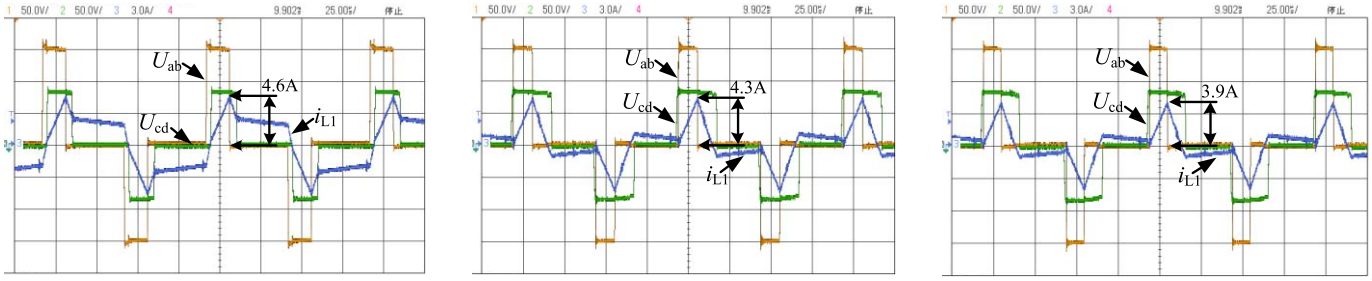

Fig. 15. Experimental waveforms of ac output voltage and inductor current under three control schemes (U_{ab}: 50 V/div, U_{cd}: 50 V/div, i_{L1}: 3 A/div, and time: 25 μs/div). (a) CSO-DPS. (b) CSO-TPS. (c) PES-TPS.

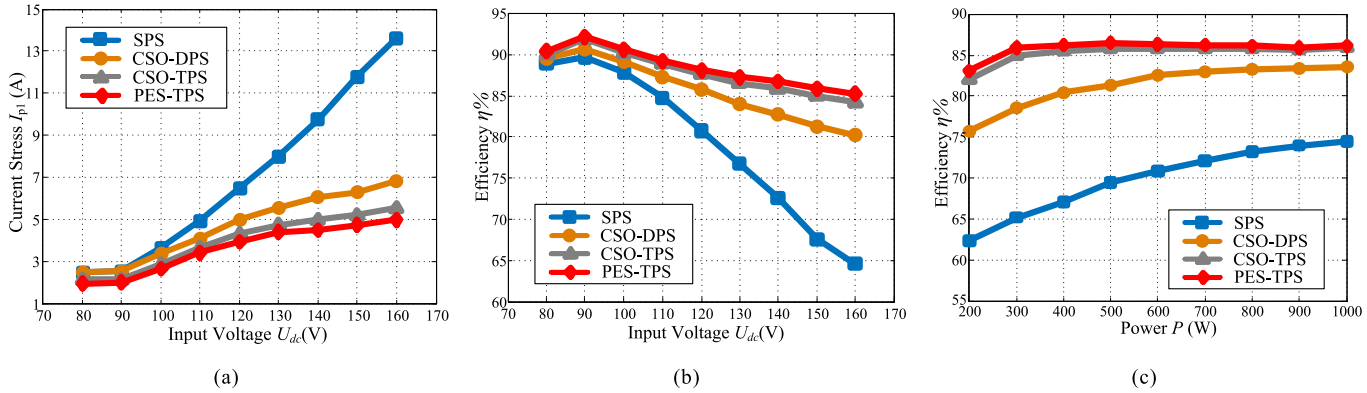

Fig. 16. Experimental waveforms of current stress and efficiency under SPS, CSO-DPS, CSO-TPS, and PES-TPS controls. (a) Current stress versus input voltage. (b) Efficiency versus input voltage. (c) Efficiency versus power ($k_i = 2$).

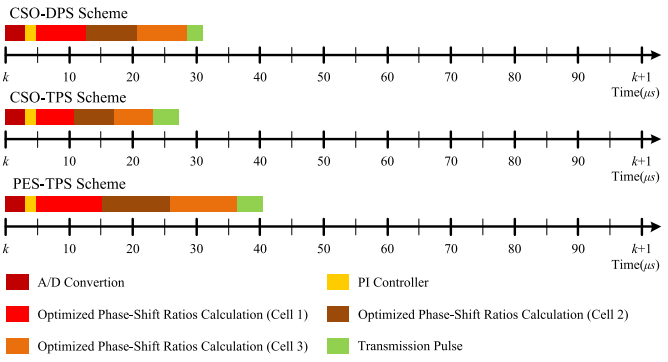

Fig. 17. Experimental comparison of real-time implementation details under CSO-DPS, CSO-TPS, and the proposed PES-TPS controls during a sampling period.

proposed scheme is about 10.9 μs, which is a little bit longer than the other two optimization schemes (8.6 μs in the CSO-DPS scheme and 6.1 μs in the CSO-TPS scheme). In addition, the total computing time of the proposed optimization scheme is about 40.2 μs.

Finally, a comprehensive performance comparison of CSO-DPS, CSO-TPS, and the proposed PES-TPS controls is concluded in Table II.

It can be seen that among the three optimization schemes, the proposed PES-TPS control can realize the converters with the most excellent dynamic performance, the highest efficiency, and the widest power balance range.

TABLE II
COMPREHENSIVE PERFORMANCE COMPARISON OF CSO-DPS, CSO-TPS, AND PROPOSED PES-TPS CONTROLS

Control Schemes / Performance	CSO-DPS	CSO-TPS	PES-TPS
Dynamic response	General	General	Excellent
Efficiency	Low	High	Higher
Power balance range	None	Partial	Wide
Computational burden	Easy	Easier	Easy

VI. CONCLUSION

This paper proposes a simple PES with TPS control to improve the efficiency, enhance the dynamic response, and balance the transmission power for the input-independent output-parallel DAB dc–dc converter in PETT. By combining the CSO and transmission power compensation, the efficiency and dynamic response of the output parallel DAB dc–dc converters can be improved simultaneously. Meanwhile, the power estimation based on operational parameters is introduced in the PES-TPS scheme to balance the transmission power over full power range. A comprehensive experimental test is adopted to compare the performance of the CSO-DPS control, the CSO-TPS control, and the proposed PES-TPS control, and the conducted studies can be concluded as follows.

1) When the traditional CSO-DPS and CSO-TPS control schemes for single DAB converter are extended into the output-parallel DAB converters in PETT, these schemes lack power balancing ability of each cell. But the proposed PES-TPS control can balance the transmission power of all DAB cells over full power range.
2) Compared to CSO-DPS and CSO-TPS control schemes, the proposed PES-TPS control can enhance the dynamic response of the output voltage under the input voltage fluctuation and load disturbance conditions, and the output voltage is almost kept constant when the input voltage or load steps change.
3) Compared to CSO-DPS and CSO-TPS control schemes, the proposed PES-TPS control can further boost the efficiency of the output-parallel DAB converter system.
4) The proposed PES-TPS control is simple and easy to be implemented in the digital controller, and it is suitable to be applied to DAB converters with the cascaded structure.

REFERENCES

[1] M. Marchesoni, R. Novaro, and S. Savio, "AC locomotive conversion systems without heavy transformers: Is it a practicable solution," in *Proc. IEEE Int. Symp. Ind. Electron.*, L'Aquila, Italy, Jul. 2002, pp. 1172–1177.

[2] B. Sun, M. Li, and A. Chao, "Research on key technology of high-speed train energy consumption," *Eng. Sci.*, vol. 17, no. 4, pp. 69–82, Apr. 2015.

[3] J. Feng, W. Q. Chu, Z. Zhang, and Z. Q. Zhu, "Power electronic transformer-based railway traction systems: Challenges and opportunities," *IEEE J. Emerg. Sel. Topics Power Electron.*, vol. 5, no. 3, pp. 1237–1253, Sep. 2017.

[4] J. Liu, J. Yang, J. Zhang, Z. Nan, and Q. Zheng, "Voltage balance control based on dual active bridge DC/DC converters in a power electronic traction transformer," *IEEE Trans. Power Electron.*, vol. 33, no. 2, pp. 1696–1714, Feb. 2018.

[5] M. Steiner and H. Reinold, "Medium frequency topology in railway applications," in *Proc. Eur. Conf. Power Electron. Appl.*, Aalborg, Denmark, 2007, pp. 1–10.

[6] M. Glinka and R. Marquardt, "A new AC/AC multilevel converter family," *IEEE Trans. Ind. Electron.*, vol. 52, no. 3, pp. 662–669, Jun. 2005.

[7] G. Wang *et al.*, "Comparisons of different control strategies for 20 kVA solid state transformer," in *Proc. IEEE Energy Convers. Congr. Expo.*, Phoenix, AZ, USA, Sep. 2011, pp. 3173–3178.

[8] P. Zumel *et al.*, "Modular dual-active bridge converter architecture," *IEEE Trans. Ind. Appl.*, vol. 52, no. 3, pp. 2444–2455, May/Jun. 2016.

[9] X. She, A. Q. Huang, and X. Ni, "Current sensorless power balance strategy for DC/DC converters in a cascaded multilevel converter based solid state transformer," *IEEE Trans. Power Electron.*, vol. 29, no. 1, pp. 17–22, Jan. 2014.

[10] S. Inoue and H. Akagi, "A bidirectional DC–DC converter for an energy storage system with galvanic isolation," *IEEE Trans. Power Electron.*, vol. 22, no. 6, pp. 2299–2306, Nov. 2007.

[11] S. Inoue and H. Akagi, "A bidirectional isolated DC–DC converter as a core circuit of the next-generation medium-voltage power conversion system," *IEEE Trans. Power Electron.*, vol. 22, no. 2, pp. 535–542, Mar. 2007.

[12] B. Zhao, S. Qiang, W. Liu, and Y. Sun, "Overview of dual-active-bridge isolated bidirectional DC-DC converter for high-frequency-link power-conversion system," *IEEE Trans. Power Electron.*, vol. 29, no. 8, pp. 4091–4106, Aug. 2014.

[13] H. Bai and C. Mi, "Eliminate reactive power and increase system efficiency of isolated bidirectional dual-active-bridge DC-DC converters using novel dual-phase-shift control," *IEEE Trans. Power Electron.*, vol. 23, no. 6, pp. 2905–2914, Nov. 2008.

[14] B. Zhao, Q. Yu, and W. Sun, "Extended-phase-shift control of isolated bidirectional DC-DC converter for power distribution in microgrid," *IEEE Trans. Power Electron.*, vol. 27, no. 11, pp. 4667–4680, Nov. 2012.

[15] A. Tong, L. Hang, G. Li, X. Jiang, and S. Gao, "Modeling and analysis of a dual-active-bridge-isolated bidirectional DC/DC converter to minimize RMS current with whole operating range," *IEEE Trans. Power Electron.*, vol. 33, no. 6, pp. 5302–5316, Jun. 2018, doi: 10.1109/TPEL.2017.2692276.

[16] Y. Shi, R. Li, Y. Xue, and H. Li, "Optimized operation of current-fed dual active bridge DC-DC converter for PV applications," *IEEE Trans. Ind. Electron.*, vol. 62, no. 11, pp. 6986–6995, Nov. 2015.

[17] B. Zhao, Q. Song, and W. Liu, "Efficiency characterization and optimization of isolated bidirectional DC–DC converter based on dual-phase-shift control for DC distribution application," *IEEE Trans. Power Electron.*, vol. 28, no. 4, pp. 1711–1727, Apr. 2013.

[18] B. Zhao, Q. Song, W. Liu, and W. Sun, "Current-stress-optimized switching strategy of isolated bidirectional DC–DC converter with dual-phase-shift control," *IEEE Trans. Ind. Electron.*, vol. 60, no. 10, pp. 4458–4467, Oct. 2013.

[19] J. Huang, Y. Wang, Z. Li, and W. Lei, "Unified triple-phase-shift control to minimize current stress and achieve full soft-switching of isolated bidirectional DC-DC converter," *IEEE Trans. Ind. Electron.*, vol. 63, no. 7, pp. 4169–4179, Jul. 2016.

[20] N. Hou, W. Song, and M. Wu, "Minimum-current-stress scheme of dual active bridge DC–DC converter with unified phase-shift control," *IEEE Trans. Power Electron.*, vol. 31, no. 12, pp. 8552–8561, Dec. 2016.

[21] X. She, A. Q. Huang, T. Zhao, and G. Wang, "Coupling effect reduction of a voltage-balancing controller in single-phase cascaded multilevel converters," *IEEE Trans. Power Electron.*, vol. 27, no. 8, pp. 3530–3543, Aug. 2012.

[22] H. Bai, C. Mi, C. Wang, and S. Gargies, "The dynamic model and hybrid phase-shift control of a dual-active-bridge converter," in *Proc. 34th Annu. Conf. IEEE Ind. Electron.*, Orlando, FL, USA, Nov. 2008, pp. 2840–2845.

[23] H. Bai, Z. Nie, and C. C. Mi, "Experimental comparison of traditional phase-shift, dual-phase-shift, and model-based control of isolated bidirectional DC–DC converters," *IEEE Trans. Power Electron.*, vol. 25, no. 6, pp. 1444–1449, Jun. 2010.

[24] G. D. Demetriades and H.-P. Nee, "Dynamic modeling of the dual-active bridge topology for high-power applications," in *Proc. IEEE Power Electron. Spec. Conf.*, Rhodes, Greece, Jun. 2008, pp. 457–464.

[25] D. Segaran, B. P. McGrath, and D. G. Holmes, "Adaptive dynamic control of a bi-directional DC-DC converter," in *Proc. IEEE Energy Convers. Congr. Expo.*, Atlanta, GA, USA, Sep. 2010, pp. 1442–1449.

[26] D. Segaran, D. G. Holmes, and B. P. McGrath, "Enhanced load step response for a bidirectional DC–DC converter," *IEEE Trans. Power Electron.*, vol. 28, no. 1, pp. 371–379, Jan. 2013.

[27] W. Song, N. Hou, and M. Wu, "Virtual direct power control scheme of dual active bridge DC-DC converters for fast dynamic response," *IEEE Trans. Power Electron.*, vol. 33, no. 2, pp. 1750–1759, Feb. 2018.

[28] P. Lefranc, X. Jannot, and P. Dessante, "Virtual prototyping and presizing methodology for buck DC-DC converters using genetic algorithms," *IET Power Electron.*, vol. 5, no. 1, pp. 41–52, 2012.

[29] L. Meng, T. Dragicevic, J. C. Vasquez, and J. M. Guerrero, "Tertiary and secondary control levels for efficiency optimization and system damping in droop controlled DC–DC converters," *IEEE Trans. Smart Grid*, vol. 6, no. 6, pp. 2615–2626, Nov. 2015.

[30] H. Zhang, X. Tong, and J. Yin, "Optimal triple-phase-shift controller design of isolated bidirectional DC-DC converter based on ant colony algorithm and BP neural network," in *Proc. 43rd Annu. Conf. IEEE Ind. Electron. Soc. (IECON)*, Beijing, China, Oct./Nov. 2017, pp. 8802–8807.

Feng An was born in Zhoukou, Henan, China, in 1994. He received the B.S. degree in electrical engineering from Southwest Jiaotong University, Chengdu, China, in 2016, where he is currently pursuing the M.S. degree in electronic engineering.

His current research interests include optimization control methods of power electronic transformers and dc distribution system.

Wensheng Song (M'13) received the B.S. degree in electronic and information engineering and the Ph.D. degree in electrical engineering from Southwest Jiaotong University, Chengdu, China, in 2006 and 2011, respectively.

From 2009 to 2010, he was a Visiting Scholar with the Department of Electrical Engineering and Computer Science, University of California, Irvine, CA, USA. In 2015, he joined the University of Alberta, Edmonton, AB, Canada, as a Visiting Scholar. He is currently an Associate Professor with the School of Electrical Engineering, Southwest Jiaotong University. His current research interests include digital control and modulation methods of electrical ac–dc–ac railway traction drive systems, and multilevel converters.

Kexin Yang was born in Meishan, Sichuan, China, in 1994. He received the B.S. degree in electrical engineering from Southwest Jiaotong University, Chengdu, China, in 2016, where he is currently pursuing the M.S. degree in electrical engineering.

His current research interests include digital control and optimization methods of dc–dc converter and dc distribution system.

Shunfeng Yang (S'15) received the B.Eng. and M.Sc. degrees in electrical engineering from Southwest Jiaotong University, Chengdu, China, in 2007 and 2010, respectively, and the Ph.D. degree in power engineering from Nanyang Technological University, Singapore, in 2018.

He is currently with the School of Electrical Engineering, Southwest Jiaotong University. His current research interests include power electronics, multilevel converters, and converter control techniques.

Lei Ma (M'08) received the Dorktor Ingenieur degree in electrical engineering from Ruhr University Bochum, Bochum, Germany, in 2006.

From 2006 to 2009, he was an Assistant Professor with the Department of Robotics and Telematics, University of Würzburg, Würzburg, Germany. From 2007 to 2009, he served as the Deputy Director and a member for the Advisory Board of the Zentrum für Telematik e.V., Würzburg. In 2009, he joined Southwest Jiaotong University, Chengdu, China, where he is currently a Full Professor. His current research interests include control theory with applications to robotic, rail-transit, and renewable energy systems.

Dr. Ma is a member of the Technical Committee of Control Theory and the Technical Committee of Cognitive Computing and Systems of Chinese Association of Automation, and a Vice Chair of IFAC TC3.3.